

NNLO+PS with MiNNLO_{PS}: status and prospects

Luca Buonocore^(a), Mauro Chiesa^(b), Gabriël Koole^(c), Daniele Lombardi^(c), Javier Mazzitelli^(c), Pier Francesco Monni^(d), Paolo Nason^(c,e), Emanuele Re^(e,f), Luca Rottoli^(a), Marius Wiesemann^(c), Giulia Zanderighi^(c), Silvia Zanolì^(c)

^(a) University of Zürich, Winterthurerstrasse 190, 8057 Zürich, Switzerland

^(b) Università di Pavia and INFN, Sezione di Pavia, Via A. Bassi 6, 27100 Pavia, Italy

^(c) Max-Planck-Institut für Physik, Föhringer Ring 6, 80805 München, Germany

^(d) CERN, Theoretical Physics Department, CH-1211 Geneva 23, Switzerland

^(e) Università di Milano - Bicocca and INFN, Sezione di Milano - Bicocca, Piazza della Scienza 3, 20126 Milano, Italy

^(f) LAPTh, Université Grenoble Alpes, USMB, CNRS, 74940 Annecy, France

Abstract

We summarize the current status and near future prospects for next-to-next-to-leading order calculations matched to parton shower based on the MiNNLO_{PS} method. We give a theoretical overview, illustrate selected results for $ZZ \rightarrow 4\ell$ and top-pair production processes at the LHC, and provide an outlook of the future challenges.

1 Introduction

The developments in the theoretical description of collider physics processes have seen a steady improvement in the precision of perturbative calculations, also matched to parton shower simulations. While twenty years ago the standard of Monte Carlo event simulations was just leading order (LO), today it is instead next-to-leading-order (NLO). However, the requirement to match the precision of LHC measurements, often reaching percent-level precision, has fostered developments towards the next-to-next-to-leading order (NNLO) level. Ten years have passed since the very first NNLO+parton shower (NNLOPS) implementations for Higgs and Drell-Yan production appeared, and new methods have been proposed which allowed a leap in the complexity of the processes that can be described. It is not unlikely that by the time the high-luminosity program will start, NNLOPS will constitute the new precision standard, together with an improved precision of the logarithmic accuracy in the parton shower to full next-to-leading-logarithmic (NLL) or even next-to-next-to-leading-logarithmic (NNLL).

The consistent combination of next-to-next-to-leading order (NNLO) QCD calculations with parton-shower simulations (NNLO+PS) is one of the current challenges in collider theory, and it is indispensable to provide the interface between accurate theory predictions and precision measurements. A good NNLO+PS method should attain NNLO accuracy for observables inclusive in the QCD radiation beyond the Born level, while preserving the logarithmic structure (and accuracy) of the parton-shower simulation after matching.

In Ref. [1, 2] we have presented the method `MINNLOPS`, which is an extension of the `MINLO'` procedure of Refs. [3, 4]. The latter method was used to obtain NNLOPS accuracy using a reweighting procedure. It was applied to some simple LHC processes, namely Higgs-boson production [5], the Drell-Yan process [6] and Higgs to bottom quark decays [7], and more complicated LHC processes, such as the two Higgs-strahlung reactions [8, 9], and the production of two opposite-charge leptons and two neutrinos (W^+W^-) [10]. These computations have employed the reweighting procedure to its extreme. In contrast, the new `MINNLOPS` procedure of Ref. [1, 2] addresses more directly the requirement of NNLO accuracy and thus, besides not using any reweighting, it can be more easily generalized to processes beyond massive colour-singlet production. It meets the following features:

- NNLO corrections are calculated directly during the generation of the events and without any additional a-posteriori reweighting.
- No merging scale is required to separate different multiplicities in the generated event samples.
- The matching to the parton shower is performed according to the `POWHEG` method [11–13] and preserves the leading logarithmic (LL) structure of transverse-momentum ordered showers.¹

This method, that up to now has been applied to the production of colour singlet system such as $Z\gamma$ [15, 16], W^+W^- [17], ZZ [18], VH including the $H \rightarrow b\bar{b}$ decay at NNLOPS [19], was extended to deal with the production of massive coloured final states in Refs. [20, 21], where it was applied to top-quark pair production. This was the first NNLOPS result for LHC processes with colored final states.

In this manuscript we first give an overview of the theoretical aspects at the core of `MINNLOPS` NNLO+PS simulations. We then discuss selected results for ZZ and $t\bar{t}$ production, and conclude with an outlook of possible future developments.

2 Theoretical overview

2.1 `MINNLOPS` in a nutshell

The `MINNLOPS` method [1, 2] formulates a NNLO calculation fully differential in the phase space Φ_F of the produced colour singlet F with invariant mass Q . It starts from a differential description of the production of the colour singlet and a jet (FJ), whose phase space we denote by Φ_{FJ} . It is described by the following formula:

$$\frac{d\sigma}{d\Phi_{FJ}} = \bar{B}(\Phi_{FJ}) \times \left\{ \Delta_{\text{pwg}}(\Lambda_{\text{pwg}}) + \int d\Phi_{\text{rad}} \Delta_{\text{pwg}}(p_{T,\text{rad}}) \frac{R(\Phi_{FJ}, \Phi_{\text{rad}})}{B(\Phi_{FJ})} \right\}, \quad (1)$$

¹For a different ordering variable, preserving the accuracy of the shower is more subtle. Not only one needs to veto shower radiation that has relative transverse momentum greater than the one generated by `POWHEG`, but also one has to resort to truncated showers [11, 14] to compensate for missing collinear and soft radiation. Failing to do so spoils the shower accuracy at leading-logarithmic level (in fact, at the double-logarithmic level).

which corresponds precisely to a standard POWHEG calculation [11–13] for FJ production, supplemented with a modified $\bar{B}(\Phi_{\text{FJ}})$ function that is crucial to reach NNLO accuracy in the production of the system F. The function $\bar{B}(\Phi_{\text{FJ}})$ describes the generation of the first radiation, while the content of the curly brackets describes the generation of the second radiation according to the POWHEG method [11–13]. Here, B and R are the squared tree-level matrix elements for FJ and FJJ production, respectively. Δ_{pwg} denotes the POWHEG Sudakov form factor [11] and $\Phi_{\text{rad}}(p_{\text{T,rad}})$ is the phase space (transverse momentum) of the second radiation, which is generated above the POWHEG infrared cutoff $\Lambda_{\text{pwg}} = 0.89$ GeV. The parton shower then adds additional radiation to the partonic events generated according to Eq. (1), and it contributes beyond $\mathcal{O}(\alpha_S^2(Q))$ at all orders in perturbation theory.

The function $\bar{B}(\Phi_{\text{FJ}})$ is the central ingredient of `MinNLOPS`. Its derivation [1] stems from the observation that the NNLO cross section differential in the transverse momentum of the color singlet (p_{T}) and in the Born phase space Φ_{F} is described by the following formula

$$\frac{d\sigma}{d\Phi_{\text{F}}dp_{\text{T}}} = \frac{d}{dp_{\text{T}}} \left\{ \exp[-\tilde{S}(p_{\text{T}})] \mathcal{L}(p_{\text{T}}) \right\} + R_f(p_{\text{T}}) = \exp[-\tilde{S}(p_{\text{T}})] \left\{ D(p_{\text{T}}) + \frac{R_f(p_{\text{T}})}{\exp[-\tilde{S}(p_{\text{T}})]} \right\}, \quad (2)$$

where R_f contains terms that are integrable in the $p_{\text{T}} \rightarrow 0$ limit, and

$$D(p_{\text{T}}) \equiv -\frac{d\tilde{S}(p_{\text{T}})}{dp_{\text{T}}} \mathcal{L}(p_{\text{T}}) + \frac{d\mathcal{L}(p_{\text{T}})}{dp_{\text{T}}}. \quad (3)$$

$\tilde{S}(p_{\text{T}})$ represents the Sudakov form factor, while $\mathcal{L}(p_{\text{T}})$ contains the parton luminosities, the squared virtual matrix elements for the underlying F production process up to two loops as well as the NNLO collinear coefficient functions. Explicit expressions can be found in Ref. [1, 2]. A crucial feature of the `MinNLOPS` method is that the renormalisation and factorisation scales are set to $\mu_{\text{R}} \sim \mu_{\text{F}} \sim p_{\text{T}}$.

Introducing the NLO differential cross section for FJ production

$$\frac{d\sigma_{\text{FJ}}^{(\text{NLO})}}{d\Phi_{\text{F}}dp_{\text{T}}} = \frac{\alpha_{\text{S}}(p_{\text{T}})}{2\pi} \left[\frac{d\sigma_{\text{FJ}}}{d\Phi_{\text{F}}dp_{\text{T}}} \right]^{(1)} + \left(\frac{\alpha_{\text{S}}(p_{\text{T}})}{2\pi} \right)^2 \left[\frac{d\sigma_{\text{FJ}}}{d\Phi_{\text{F}}dp_{\text{T}}} \right]^{(2)}, \quad (4)$$

where $[X]^{(i)}$ denotes the coefficient of the i -th term in the perturbative expansion of the quantity X , one can rewrite Eq. (2) as

$$\begin{aligned} \frac{d\sigma}{d\Phi_{\text{F}}dp_{\text{T}}} = \exp[-\tilde{S}(p_{\text{T}})] & \left\{ \frac{\alpha_{\text{S}}(p_{\text{T}})}{2\pi} \left[\frac{d\sigma_{\text{FJ}}}{d\Phi_{\text{F}}dp_{\text{T}}} \right]^{(1)} \left(1 + \frac{\alpha_{\text{S}}(p_{\text{T}})}{2\pi} [\tilde{S}(p_{\text{T}})]^{(1)} \right) + \left(\frac{\alpha_{\text{S}}(p_{\text{T}})}{2\pi} \right)^2 \left[\frac{d\sigma_{\text{FJ}}}{d\Phi_{\text{F}}dp_{\text{T}}} \right]^{(2)} \right. \\ & \left. + \left[D(p_{\text{T}}) - \frac{\alpha_{\text{S}}(p_{\text{T}})}{2\pi} [D(p_{\text{T}})]^{(1)} - \left(\frac{\alpha_{\text{S}}(p_{\text{T}})}{2\pi} \right)^2 [D(p_{\text{T}})]^{(2)} \right] + \text{regular terms of } \mathcal{O}(\alpha_{\text{S}}^3) \right\}. \quad (5) \end{aligned}$$

The NNLO fully differential cross section is then obtained upon integration over p_{T} from scales of the order of the Landau pole Λ to the kinematic upper bound. Each term in Eq. (5) contributes to the total cross section according to the power counting formula

$$\int_{\Lambda}^Q dp_{\text{T}} \frac{1}{p_{\text{T}}} \alpha_{\text{S}}^m(p_{\text{T}}) \ln^n \frac{Q}{p_{\text{T}}} \exp(-\tilde{S}(p_{\text{T}})) \approx \mathcal{O} \left(\alpha_{\text{S}}^{m-\frac{n+1}{2}}(Q) \right), \quad (6)$$

which clarifies why certain terms of $\mathcal{O}(\alpha_s^3)$ should be included.

The above considerations can be made at the fully differential level on the Φ_{FJ} phase space, which leads to the definition of the $\bar{B}(\Phi_{\text{FJ}})$ function as [1]

$$\begin{aligned} \bar{B}(\Phi_{\text{FJ}}) \equiv \exp[-\tilde{S}(p_{\text{T}})] & \left[B(\Phi_{\text{FJ}}) \left(1 + \frac{\alpha_s(p_{\text{T}})}{2\pi} [\tilde{S}(p_{\text{T}})]^{(1)} \right) + V(\Phi_{\text{FJ}}) \right. \\ & \left. + D(p_{\text{T}})^{(\geq 3)} F^{\text{corr}}(\Phi_{\text{FJ}}) \right] + \int d\Phi_{\text{rad}} R(\Phi_{\text{FJ}}, \Phi_{\text{rad}}) \tilde{S}(p_{\text{T}}), \end{aligned} \quad (7)$$

where $D(p_{\text{T}})^{(\geq 3)}$ corresponds to the square bracket in the second line of Eq. (5), and the factor $F^{\text{corr}}(\Phi_{\text{FJ}})$ encodes its dependence upon the full Φ_{FJ} phase space, as discussed in detail in Section 3 of Ref. [1].

2.2 Extension beyond the colour singlet case

In the case of the production of coloured final states, such as top-quark pair production, the starting point to derive the singular term in Eq. (2) is the more complex expression

$$\sum_{c=\bar{q}, \bar{q}, g} \frac{|M_{c\bar{c}}^{(0)}|^2}{2m_{t\bar{t}}^2} \int \frac{d^2\vec{b}}{(2\pi)^2} e^{i\vec{b}\cdot\vec{p}_{\text{T}}} e^{-S_c(\frac{b_0}{b})} \times \sum_{i,j} \text{Tr}(\mathbf{H}_c \mathbf{\Delta}) (C_{ci} \otimes f_i) (C_{\bar{c}j} \otimes f_j), \quad (8)$$

which describes the production of a pair of heavy quarks at small transverse momentum. Here $b_0 = 2e^{-\gamma_E}$, $b = |\vec{b}|$. S_c is the same Sudakov radiator which also enters the description of the production of a colour singlet system at small transverse momentum. The first sum in Eq. (8) runs over all possible flavour configurations of the incoming partons p_1 of flavour c and p_2 of flavour \bar{c} . The collinear coefficient functions $C_{ij} = C_{ij}(z, p_1, p_2, \vec{b}; \alpha_s(b_0/b))$ describe the structure of constant terms related to the emission of collinear radiation, and the parton densities are denoted by f_i and are evaluated at b_0/b . The operation \otimes denotes the standard convolution over the momentum fraction z carried by initial state radiation. The factor $\text{Tr}(\mathbf{H}_c \mathbf{\Delta}) (C_{ci} \otimes f_i) (C_{\bar{c}j} \otimes f_j)$ has different expressions for the $q\bar{q}$ and gg channels and has here a symbolic meaning. In particular, it has a rich Lorentz structure that we omit for simplicity, which is a source of azimuthal correlations in the collinear limit [22, 23].

All quantities in bold face denote operators in colour space, and the trace $\text{Tr}(\mathbf{H}_c \mathbf{\Delta})$ in Eq. (8) runs over the colour indices. The hard function $\mathbf{H}_c = \mathbf{H}_c(\Phi_{t\bar{t}}; \alpha_s(m_{t\bar{t}}))$ is obtained from the subtracted amplitudes and the ambiguity in its definition corresponds to using a specific resummation scheme [24]. The operator $\mathbf{\Delta}$ encodes the structure of the quantum interference due to the exchange of soft radiation at large angle between the initial and final state, and within the final state. It is given by $\mathbf{\Delta} = \mathbf{V}^\dagger \mathbf{D} \mathbf{V}$, where [23]

$$\mathbf{V} = \mathcal{P} \exp \left\{ - \int_{b_0^2/b^2}^{m_{t\bar{t}}^2} \frac{dq^2}{q^2} \mathbf{\Gamma}_t(\Phi_{t\bar{t}}; \alpha_s(q)) \right\}. \quad (9)$$

The symbol \mathcal{P} denotes the path ordering (with increasing scales from left to right) of the exponential matrix with respect to the integration variable q^2 . $\mathbf{\Gamma}_t$ is the anomalous dimension accounting for

the effect of real soft radiation at large angles, and $\mathbf{D} = \mathbf{D}(\Phi_{t\bar{t}}, \vec{b}; \alpha_s(b_0/b))$ encodes the azimuthal dependence of the corresponding constant terms, and is defined such that $[\mathbf{D}]_\phi = \mathbf{1}$, where $[\dots]_\phi$ denotes the average over the azimuthal angle ϕ of \vec{p}_T .

The strategy to arrive at a `MinNLOPS` improved \bar{B} function is the same as for the colour-singlet case. We expand Eq. (8) taking care of not spoiling the NNLO counting accuracy outlined in Eq. (6) and maintaining leading logarithmic accuracy to arrive to an expression in transverse momentum space that can be used to correct the \bar{B} function in order to achieve NNLO accuracy. All details are given in Refs. [20, 21].

3 Selected results

Here, as an example, we discuss selected results for ZZ and $t\bar{t}$ production. The uncertainty bands shown are in general obtained with a standard seven-point scale variation of renormalisation and factorisation scales, and possibly with a variation of the resummation scale, as described in the relevant publications.

3.1 ZZ production

The accurate simulation of the production of a pair of Z bosons, with subsequent decay into a four-lepton final state, is instrumental for the precision program of the LHC. This process constitutes a relevant background in Higgs boson measurements, and plays an important role in constraining the presence of anomalous interactions in the gauge sector of the Standard Model. Accordingly, an accurate event generation is of paramount importance. In this section we present some sample `MinNLOPS` results for this process.

Fig. 1 displays predictions for the transverse momentum of the diboson pair ($p_{T,4\ell}$). We show `MinNLOPS` predictions (purple), compared to `MinLO'` results (red). The latter is only NLO accurate, and fixed-order NNLO predictions from `Matrix` [26] (green). We also show the NNLO+N³LL result obtained with `Matrix+RadISH` [25] (blue), which interfaces `Matrix` to the `RadISH` resummation formalism [27, 28]. Since `Matrix+RadISH` does not include the contribution stemming from the loop-induced gg channel, we perform this comparison by considering in our `MinNLOPS` result only the $q\bar{q}$ -initiated process, i.e. at the NNLO _{$q\bar{q}$} +PS level. At small values of the ZZ transverse momentum we observe an excellent agreement between the NNLO+N³LL and the `MinNLOPS` result, especially considering the lower accuracy of the parton shower in that region; `MinNLOPS` is between 5% and 12% larger than the NNLO+N³LL prediction below 10 GeV and has a larger uncertainty band reflecting its lower accuracy. On the other hand, the `MinLO'` result is $\mathcal{O}(10\%)$ smaller than the NNLO+N³LL and the `MinNLOPS` predictions, and its uncertainty band does not overlap with either of the more accurate results below 40 GeV. Fixed-order calculations actually lead to unphysical results in the small- $p_{T,4\ell}$ region due to large logarithmic corrections, which need to be resummed to all orders. Indeed, the NNLO result diverges at low transverse momentum, and its prediction differs significantly from the ones including resummation effects. At larger values of $p_{T,4\ell}$ the NNLO result is instead in agreement with the NNLO+N³LL, `MinLO'` and `MinNLOPS` predictions, as one may expect since all of them have the same formal accuracy in the tail of the distribution.

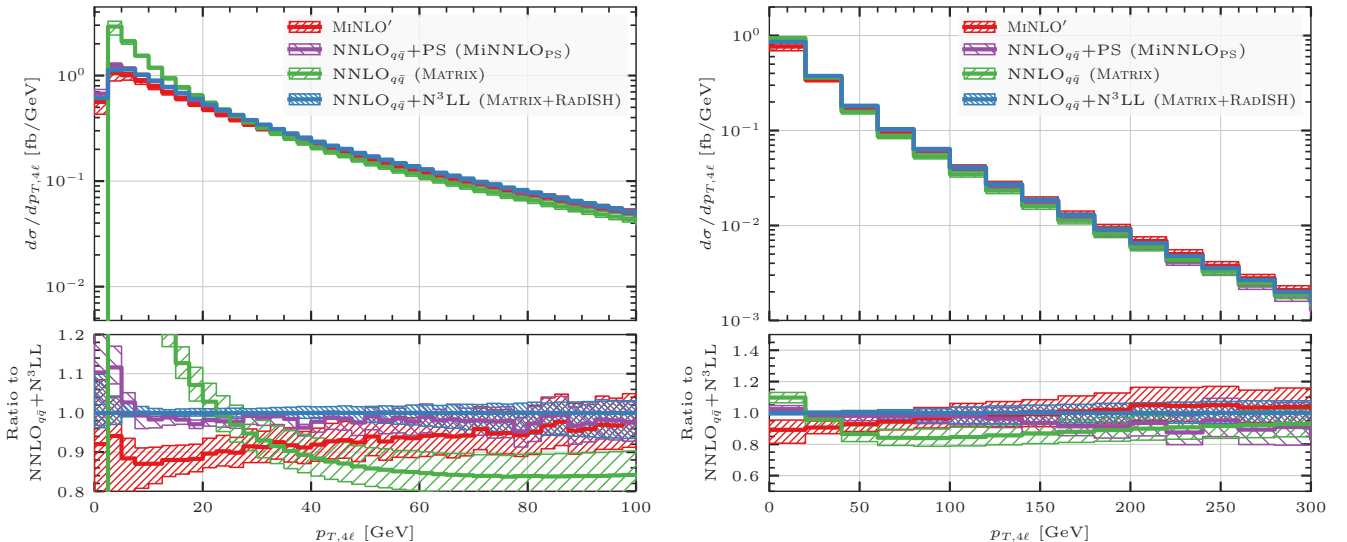


Figure 1: Comparison between NNLO (Matrix), MiNLO', MiNNLO_{PS} and the NNLO+N³LL of Matrix+RadISH [25] for the transverse momentum of the ZZ pair for two different ranges of $p_{T,4\ell}$. Figure taken from Ref. [18].

Next we show a comparison to CMS data of Ref. [29] for the invariant mass and the transverse momentum of the diboson pair ($m_{4\ell}$ and $p_{T,4\ell}$), now including also the gluon-induced production described at NLOPS accuracy. By and large, we observe a quite good agreement between our predictions and the experimental data. The invariant mass is well described at low $m_{4\ell}$, but there is a tendency of the predictions to overshoot the data at large $m_{4\ell}$, with the last bin being almost two standard deviations away. In this region electroweak (EW) corrections are known to be important and they are only partly included here through the QED shower. A simple inclusion of the NLO EW corrections, obtained via a reweighting of the events by a proper EW K-factor (see Ref. [18] for more details), can visibly improve the agreement with data in this region. The transverse-momentum distribution of the ZZ pair is also well described, except for a two-sigma deviation in the last bin, with a remarkable agreement for $p_{T,4\ell}$ values below ~ 100 GeV, where the all-order corrections provided by the shower are particularly important.

3.2 $t\bar{t}$ production

The production of a pair of top quarks enters a number of important analyses at the LHC. Due to its abundance, it is an important background to several electroweak and Higgs processes, as well as beyond the Standard Model searches. Moreover, it constitutes the main production mechanism of top quarks at the LHC, and it is therefore an ideal process to study top-quark properties accurately.

In Fig. 3, we show MiNNLO_{PS} (blue, solid), MiNLO' (gray, dotted) and fixed-order NNLO (red, dashed) predictions compared to data from CMS [30] (black points with errors) that has been extrapolated from semi-leptonic top-quark decays to the inclusive $t\bar{t}$ phase space. We show the rapidity $y_{t\bar{t}}$ and the transverse momentum of the leading top p_{T,t_1} . With respect to MiNLO', the MiNNLO_{PS} corrections lead to a significant increase of about 10% in the central value, and a substantial reduction of the scale uncertainties of more than a factor of two. We find excellent agreement between MiNNLO_{PS} and fixed-order NNLO predictions for the rapidity distribution, both

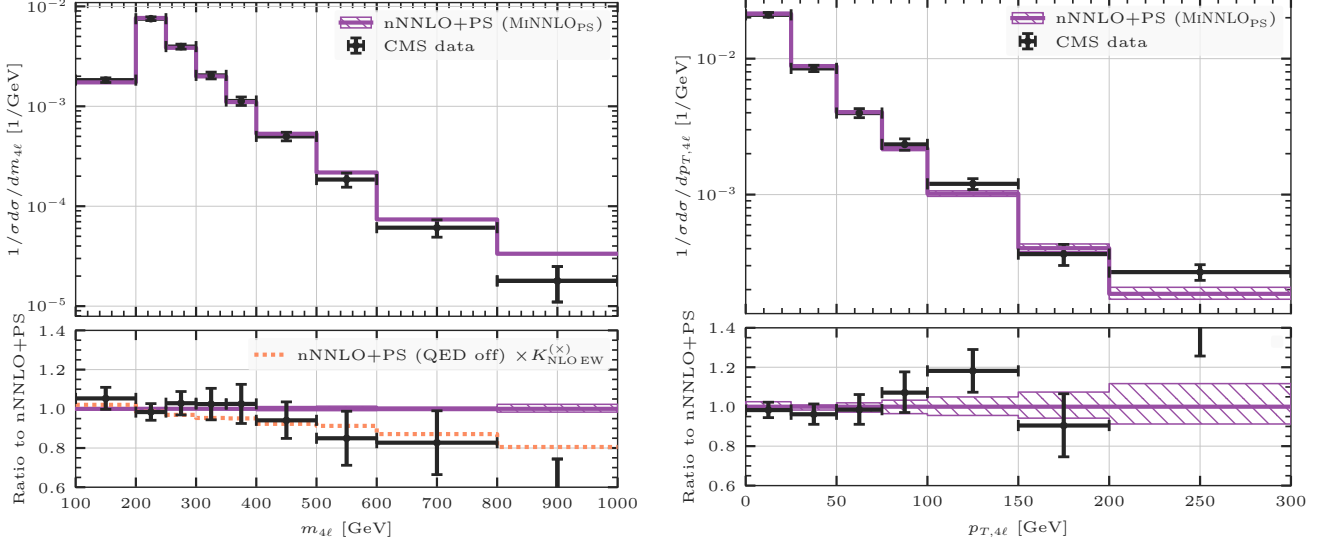


Figure 2: Comparison between the MiNNLO_{PS} predictions and the CMS data of Ref. [29] based on a 137 fb^{-1} 13 TeV analysis for $m_{4\ell}$ and $p_{T,4\ell}$. The MiNNLO_{PS} predictions include hadronization and multi-parton interactions effects, as well as QED effects as provided by the Pythia8 parton shower. Figure taken from Ref. [18].

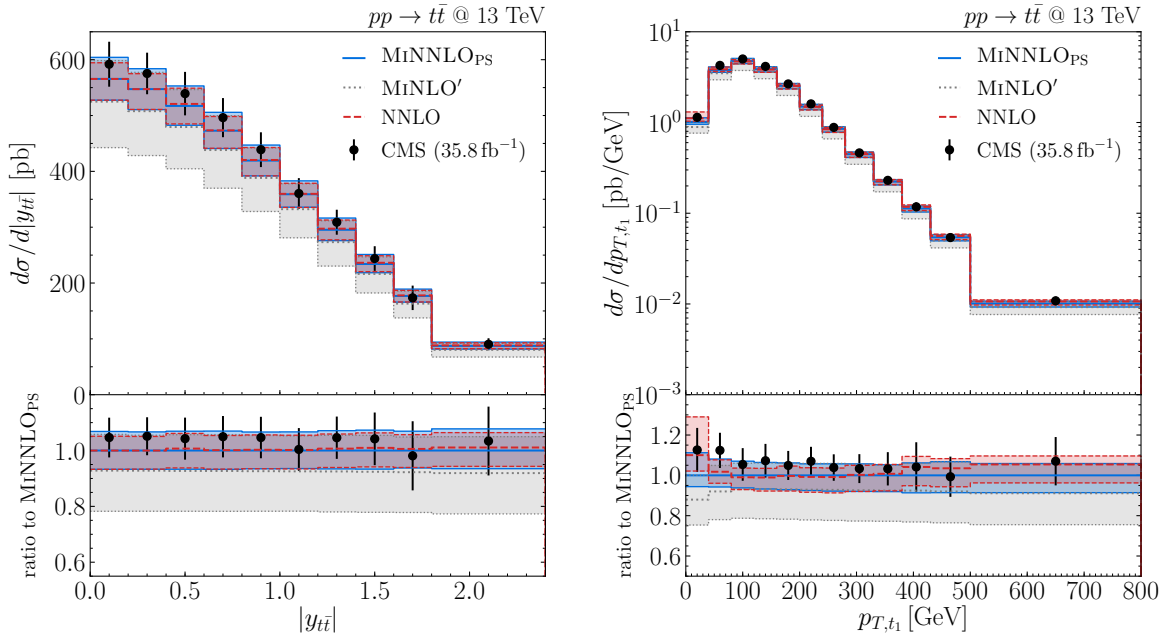


Figure 3: Comparison of MiNNLO_{PS} (blue, solid), MiNLO' (black, dashed), and NNLO QCD (red, dashed) predictions with CMS data [30] (black points with errors) with no phase space cuts. Figure taken from Ref. [21].

for the central predictions and for the scale-uncertainty bands. For the transverse momentum distribution we observe mild differences between MiNNLO_{PS} and NNLO at small p_{T,t_1} , especially in terms of shape. This is expected since this distribution is affected by large logarithmic contributions in this region, therefore a matching to the parton shower becomes particularly important. The observed differences with respect to NNLO are however largely covered by the perturbative

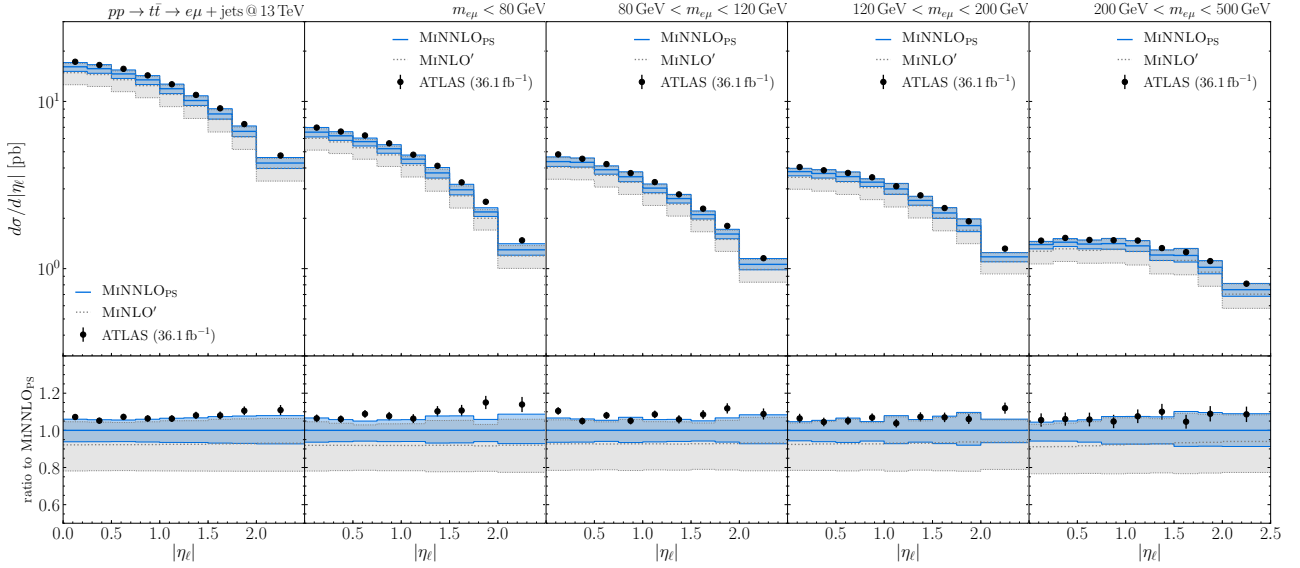


Figure 4: Comparison of $\text{MiNNLO}_{\text{PS}}$ (blue, solid) and MiNLO' (gray, dashed) predictions with ATLAS data [31] (black points with errors) in the fully leptonic decay mode, including decays of τ leptons.

uncertainties and both results are in excellent agreement with the experimental data.

We continue by considering $\text{MiNNLO}_{\text{PS}}$ predictions in comparison to data for various distributions in the phase space of the top-decay products, now including fiducial selection cuts. For simplicity, we only show the MiNLO' results as a reference prediction in the following. We start by considering the decay channel where both top quarks decay leptonically, requiring one electron and one muon in the final signature. In Figure 4 we show the rapidity of the two leptons η_ℓ (binned together), inclusively over $m_{e\mu}$ (first panel) as well as in slices of $m_{e\mu}$, as measured by ATLAS at 13 TeV [31] (black points with errors) in comparison to $\text{MiNNLO}_{\text{PS}}$ (blue, solid) and MiNLO' (gray, dotted) predictions. In the results considered here, the electrons and muons may also stem from top-quark decays to τ leptons and their subsequent leptonic decays. The shapes are described very well and the data is at the upper edge of the uncertainty band of $\text{MiNNLO}_{\text{PS}}$, but overall still compatible. Compared to the MiNLO' prediction, we observe a substantial reduction of the uncertainty band.

4 Outlook

The $\text{MiNNLO}_{\text{PS}}$ method can currently be used to describe processes with generic colour structure that, at the Born level, do not include light partons in the final state, the only requirement being the availability of the resummation of a suitable kinematic variable (such as, for instance, the transverse momentum of the heavy system) at the desired perturbative accuracy as well as the NNLO computation of the hard process. The next milestone is likely to be the matching for a process with a light parton in the final state, such as Higgs plus jet or Drell-Yan plus jet. Similarly, NLO EW corrections may compete with NNLO QCD ones and a joint inclusion of both is another important future goal. A crucial observation is that the ongoing efforts to improve the logarithmic accuracy of the shower to NLL, and eventually NNLL level, are likely to add new requirements for

NLOPS and NNLOPS methods, which at the moment only preserve the LL accuracy of the shower.

References

- [1] P. F. Monni, P. Nason, E. Re, M. Wiesemann, and G. Zanderighi, (2019), arXiv:1908.06987 [hep-ph] .
- [2] P. F. Monni, E. Re, and M. Wiesemann, Eur. Phys. J. C **80**, 1075 (2020), arXiv:2006.04133 [hep-ph] .
- [3] K. Hamilton, P. Nason, and G. Zanderighi, JHEP **10**, 155 (2012), arXiv:1206.3572 [hep-ph] .
- [4] K. Hamilton, P. Nason, C. Oleari, and G. Zanderighi, JHEP **05**, 082 (2013), arXiv:1212.4504 [hep-ph] .
- [5] K. Hamilton, P. Nason, E. Re, and G. Zanderighi, JHEP **10**, 222 (2013), arXiv:1309.0017 [hep-ph] .
- [6] A. Karlberg, E. Re, and G. Zanderighi, JHEP **09**, 134 (2014), arXiv:1407.2940 [hep-ph] .
- [7] W. Bizoń, E. Re, and G. Zanderighi, JHEP **06**, 006 (2020), arXiv:1912.09982 [hep-ph] .
- [8] W. Astill, W. Bizon, E. Re, and G. Zanderighi, JHEP **06**, 154 (2016), arXiv:1603.01620 [hep-ph] .
- [9] W. Astill, W. Bizoń, E. Re, and G. Zanderighi, JHEP **11**, 157 (2018), arXiv:1804.08141 [hep-ph] .
- [10] E. Re, M. Wiesemann, and G. Zanderighi, JHEP **12**, 121 (2018), arXiv:1805.09857 [hep-ph] .
- [11] P. Nason, JHEP **11**, 040 (2004), arXiv:hep-ph/0409146 [hep-ph] .
- [12] S. Frixione, P. Nason, and C. Oleari, JHEP **11**, 070 (2007), arXiv:0709.2092 [hep-ph] .
- [13] S. Alioli, P. Nason, C. Oleari, and E. Re, JHEP **06**, 043 (2010), arXiv:1002.2581 [hep-ph] .
- [14] M. Bahr et al., Eur. Phys. J. **C58**, 639 (2008), arXiv:0803.0883 [hep-ph] .
- [15] D. Lombardi, M. Wiesemann, and G. Zanderighi, JHEP **06**, 095 (2021), arXiv:2010.10478 [hep-ph] .
- [16] D. Lombardi, M. Wiesemann, and G. Zanderighi, Phys. Lett. B **824**, 136846 (2022), arXiv:2108.11315 [hep-ph] .
- [17] D. Lombardi, M. Wiesemann, and G. Zanderighi, JHEP **11**, 230 (2021), arXiv:2103.12077 [hep-ph] .
- [18] L. Buonocore, G. Koole, D. Lombardi, L. Rottoli, M. Wiesemann, and G. Zanderighi, JHEP **01**, 072 (2022), arXiv:2108.05337 [hep-ph] .
- [19] S. Zanolì, M. Chiesa, E. Re, M. Wiesemann, and G. Zanderighi, (2021), arXiv:2112.04168 [hep-ph] .

- [20] J. Mazzitelli, P. F. Monni, P. Nason, E. Re, M. Wiesemann, and G. Zanderighi, *Phys. Rev. Lett.* **127**, 062001 (2021), arXiv:2012.14267 [hep-ph] .
- [21] J. Mazzitelli, P. F. Monni, P. Nason, E. Re, M. Wiesemann, and G. Zanderighi, (2021), arXiv:2112.12135 [hep-ph] .
- [22] S. Catani and M. Grazzini, *Nucl. Phys.* **B845**, 297 (2011), arXiv:1011.3918 [hep-ph] .
- [23] S. Catani, M. Grazzini, and A. Torre, *Nucl. Phys.* **B890**, 518 (2014), arXiv:1408.4564 [hep-ph] .
- [24] G. Bozzi, S. Catani, D. de Florian, and M. Grazzini, *Nucl. Phys.* **B737**, 73 (2006), arXiv:hep-ph/0508068 [hep-ph] .
- [25] S. Kallweit, E. Re, L. Rottoli, and M. Wiesemann, *JHEP* **12**, 147 (2020), arXiv:2004.07720 [hep-ph] .
- [26] M. Grazzini, S. Kallweit, and M. Wiesemann, *Eur. Phys. J.* **C78**, 537 (2018), arXiv:1711.06631 [hep-ph] .
- [27] P. F. Monni, E. Re, and P. Torrielli, *Phys. Rev. Lett.* **116**, 242001 (2016), arXiv:1604.02191 [hep-ph] .
- [28] W. Bizon, P. F. Monni, E. Re, L. Rottoli, and P. Torrielli, (2017), arXiv:1705.09127 [hep-ph] .
- [29] A. M. Sirunyan et al. (CMS), *Eur. Phys. J. C* **81**, 200 (2021), arXiv:2009.01186 [hep-ex] .
- [30] A. M. Sirunyan et al. (CMS), *Phys. Rev. D* **97**, 112003 (2018), arXiv:1803.08856 [hep-ex] .
- [31] G. Aad et al. (ATLAS), *Eur. Phys. J. C* **80**, 528 (2020), arXiv:1910.08819 [hep-ex] .